Design of an aeroelastically tailored 10 MW wind turbine rotor

Zahle, Frederik; Tibaldi, Carlo; Pavese, Christian; McWilliam, Michael; Blasques, José Pedro Albergaria Amaral; Hansen, Morten Hartvig

Published in:
Journal of Physics: Conference Series (Online)

Link to article, DOI:
10.1088/1742-6596/753/6/062008

Publication date:
2016

Design of an Aeroelastically Tailored 10 MW Wind Turbine Rotor

2016 J. Phys.: Conf. Ser. 753 062008

(http://iopscience.iop.org/1742-6596/753/6/062008)

Design of an Aeroelastically Tailored 10 MW Wind Turbine Rotor

Frederik Zahle, Carlo Tibaldi, Christian Pavese, Michael K. McWilliam, Jose P. A. A. Blasques, Morten H. Hansen

DTU Wind Energy, Risø Campus, Frederiksborgvej 399, Roskilde, Denmark

E-mail: frza@dtu.dk

Abstract. This work presents an integrated multidisciplinary wind turbine optimization framework utilizing state-of-the-art aeroelastic and strutural tools, capable of simultaneous design of the outer geometry and internal structure of the blade. The framework is utilized to design a 10 MW rotor constrained not to exceed the design loads of an existing reference wind turbine. The results show that through combined geometric tailoring of the internal structure and aerodynamic shape of the blade it is possible to achieve significant passive load alleviation that allows for a 9% longer blade with an increase in AEP of 8.7%, without increasing blade mass and without significant increases in ultimate and fatigue loads on the hub and tower.

1. Introduction

Designers of modern wind turbine blades continuously push blade lengths upwards to increase the capacity factors of their rotors in order to reduce the cost of energy (CoE). In the industry it is also common to develop new blades for existing platforms, thus reducing the overall costs by enabling re-use of components such as tower, drivetrain and hub. Such a blade thus has a pre-determined loads envelope dictated by the platform it is fitted on.

Stretching the blades on a platform for the same wind climate poses several challenges both structurally, aerodynamically and aeroelastically. Structurally, longer blades require higher stiffness to maintain tower clearance, which can be achieved through increased cross-sectional thickness or more material in the blade. Increasing thickness can be achieved by increasing the chord for the same relative thickness, which, however, can increase loads. Increasing thickness through an increase in relative thickness enables a slender planform, but will generally result in lower aerodynamic efficiency. Using the same drivetrain will also place constraints on the maximum allowable rotor torque, requiring an increase in tip speed ratio, likewise driving down blade solidity. The above constraints point towards slender blade planforms combined with the use of aerofoils of higher relative thickness. Aeroelastic tailoring with which the blade twists to unload the blade can be effective to avoid increased loads or tower strike during operation due to longer blades. Torsional couplings can be introduced is different ways, e.g. with material anisotropy or blade inplane sweep. Leveraging the trade-offs and introducing aeroelastic tailoring are, however, not trivial, and to handle the myriad of conflicting objectives and constraints in the blade design process, multidisciplinary optimization techniques are broadly agreed upon to be necessary. This has been demonstrated by several authors [1, 2, 3, 4, 5].

In [6] the present authors demonstrated the use of the aero-structural design tool HAWTOpt2 in which the internal structure and the blade aerodynamic shape was designed simultaneously for a fixed blade length, constraining extreme loads of the platform not to exceed the starting point. In this article we demonstrate the capabilities of HAWTOpt2, which is a complete rewrite of the tool presented in [6], which now uses a more efficient MPI based communication that allows for parallelisation of the workflow at multiple levels, and also interfaces to the time domain aeroelastic solver HAWC2 to compute extreme loads. This has allowed us to extend the design problem to most importantly include blade length as a free parameter, with which the objective was to maximise AEP while respecting the overall loads envelope of the original DTU 10MW RWT.

2. Aerostructural Design Tool

HawtOpt2 uses OpenMDAO v1.x [7] to handle the definition of the optimization problem, workflow, dataflow and parallelization of simulation cases. This allows us to efficiently make use of high performance computing clusters, with MPI parallelisation of both cases within the objective function (e.g. design load cases), as well as the evaluation of finite difference gradients. OpenMDAO provides an interface to PyOptSparse [8] which has wrappers for several optimization algorithms. In this work, the open source gradient-based interior point optimizer IPOPT [9] is used. HawtOpt2 has interfaces to the finite element cross sectional tool BECAS [10, 11] and to the aeroelastic tools HAWC2 [12] and HAWCStab2 [13]. BECAS allows for the evaluation of the cross sectional structural and mass properties of the blade, as well as calculation of material failure both with respect to ultimate and fatigue loads. HAWCStab2 uses an unsteady blade element momentum (BEM) model of the rotor and a geometrically non-linear finite beam element model to compute steady-state aerodynamic states, structural deflections and linearized models of the wind turbine. HAWCStab2 has an analytical linearisation of the high-order aeroservoelastic model, which can be used for frequency analysis, controller tuning and evaluation of fatigue damage equivalent load rates using a frequency domain based approach [14]. Untimate loads simulations within the optimization loop are carried out using the aero-hydro-servo-elastic software package HAWC2 on a reduced set of design load cases as per IEC 61400-1 Ed3, while the final designs are evaluated using the full design load basis described in ref. [15].

Figure 1 shows a so-called extended design structure matrix diagram (XDSM) [16] of the workflow in HawtOpt2. Overlaid boxes indicate components that are executed in parallel for each cross-section/load case. At the upper level, the entire workflow is parallelised to enable parallel gradient evaluation. All of these parallelisations are embarrassingly parallel and thus this scales linearly with the number of CPUs available. A typical optimization will use 20 cores per objective function evaluation, and be parallelised according to the available resource with n number of concurrent FD gradient evaluations. For the present study 30 concurrent FD evaluations were used. A single objective evaluation required approximately 4 minutes, and therefore approximately 12 minutes per major iteration for 60 design variables, using a total of 600 cores.

3. Blade Paramerization

The blade planform is described in terms of distributions of chord, twist, relative thickness and pitch axis aft leading edge, the latter being the distance between the leading edge and the blade axis. The lofted shape of the blade is generated based on interpolation of a family of airfoils with different relative thicknesses.

The internal structure is defined from a number of regions that each cover a fraction of the cross-sections along the blade. Each region consists of a number of materials that are placed according to a certain stacking sequence. Figure 2 shows a cross section in which the

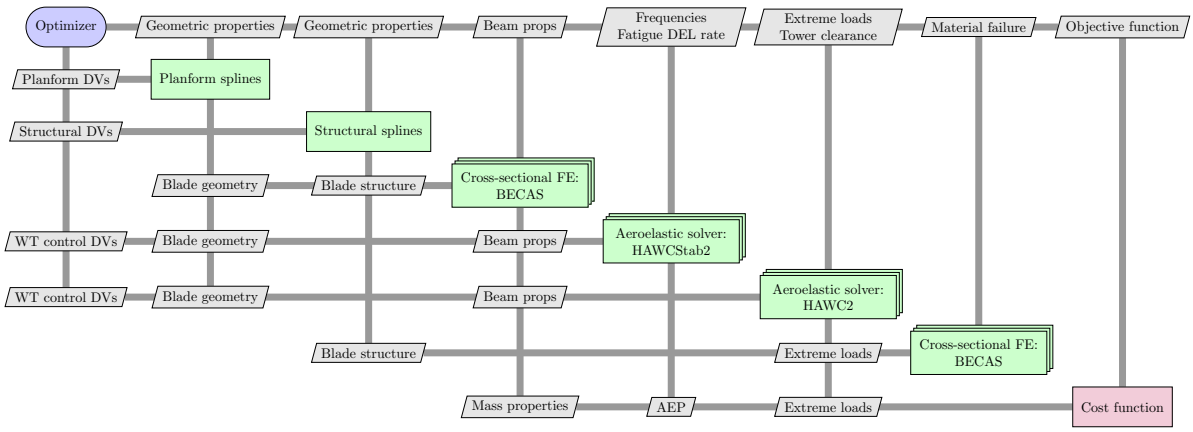

Figure 1. Extended Design Structure Matrix diagram of the workflow of HawtOpt2.

region division points (DPs) are indicated. The DP curves are described by a smooth spline as function of span that takes values between s=-1 and s=1, where s=-1 is located at the pressure side trailing edge, s=0 is at the leading edge, and s=1 is located at the trailing edge suction side. Shear webs are associated to two specific DPs on the pressure and suction side, respectively, and will move according to these points. The composite layup is likewise described by a series of smooth splines describing the thicknesses of individual layers. Fore more details on the parameterisation see [17].

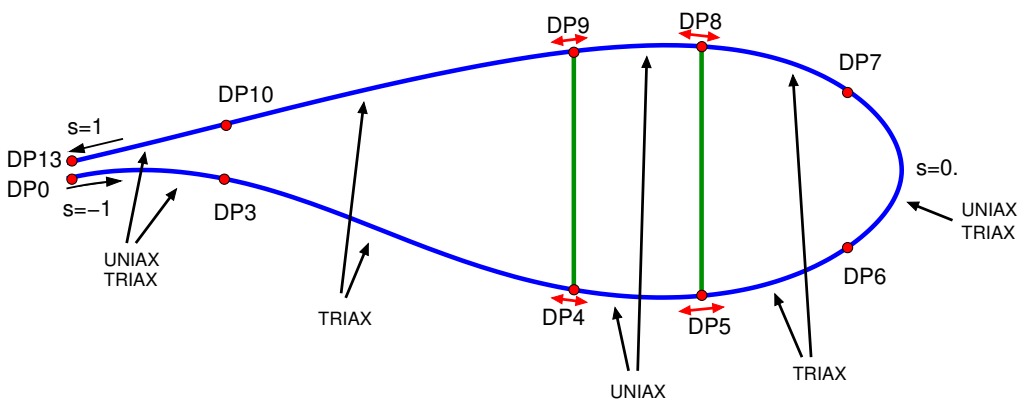

Figure 2. Region division points (DP) definition: red points indicate division points between regions; their positions are defined as curve fraction from pressure side TE (s=-1) to LE (s=0) to suction side TE (s=1).

4. Problem formulation

The numerical optimization problem that is solved is defined as:

$$\begin{aligned} \underset{\mathbf{x}_p, \mathbf{x}_s, \mathbf{x}_{oper}}{\text{minimize}} \quad & f(\{\mathbf{x}_p,\, \mathbf{x}_s\ \mathbf{x}_{oper}, \mathbf{p}, w) \\ \text{subject to} \quad & \mathbf{g}(\mathbf{x}_p) \leq \mathbf{0}, \\ & \mathbf{h_g}(\mathbf{x}_s) \leq \mathbf{0}, \\ & \mathbf{h_s}(\mathbf{x}_s) \leq \mathbf{0}, \\ & \mathbf{k}(\{\mathbf{x}_p,\, \mathbf{x}_s\}) \leq \mathbf{0} \end{aligned} \tag{1}$$

A scalar cost function f is minimized, subject to several nonlinear constraints. The cost function depends on a set of design variables $\{\mathbf{x}_p\}$, $\{\mathbf{x}_s\}$ and $\{\mathbf{x}_{oper}\}$. The design variables can be divided into three sets: the planform variables $\mathbf{x}_p$, the structural variables $\mathbf{x}_s$, and the control variables $\{\mathbf{x}_{oper}\}$. The planform variables define the outer shape of the blade. These variables are the chord, the twist, the relative thickness and pitch axis aft leading edge distributions, as well as rotor cone. The structural variables define the internal geometry of each blade blade section. These variables include thicknesses of the different material layups and position and width of the spar caps. The control variables are rotor minimum and maximum rotational speed, below rated tip speed ratio, and blade pitch. The blade pitch is optimized to track maximum power production, and controlled internally in the aeroelastic solvers. Minimum and maximum rotation speeds are fixed leaving only the tip speed ratio as a design variable. The design variables, together with the parameters $\mathbf{p}$, define the entire wind turbine.

The cost function is defined as

$$f(\{\mathbf{x}_p,\, \mathbf{x}_s,\, \mathbf{x}_{oper}\}, \mathbf{p}) = -\frac{AEP(\{\mathbf{x}_p,\, \mathbf{x}_s,\, \mathbf{x}_{oper}\}, \mathbf{p})}{AEP(\{\mathbf{0},\, \mathbf{0},\, \mathbf{0}\}, \mathbf{p})} \tag{2}$$

AEP is the annual energy production and $AEP(\{\mathbf{0},\, \mathbf{0}, \mathbf{0}\}, \mathbf{p})$ is the annual energy production of the baseline design. Three different types of constraints are defined depending on the variables they depend on. Constraints $\mathbf{g}$ depend only on planform parameters. They include bounds on the chord and relative thickness. Constraints $\mathbf{h_g}$ depends only on structural parameters. These constraints include bounds on the material thicknesses and on the position and widths of the spar caps. Constraints $\mathbf{h_s}$ denote the limits on the maximum allowable stresses in the structure. The constraints $\mathbf{k}$ depend on both the planform and structural variables, such as blade tip deflection and loads.

Tables 1 and 2 provides a summary of design variables and constraints used in this study.

Although possible in the design tool, we have in this work not applied constraints on system natural frequencies, which could lead to instabilities under high turbulence conditions. Work is under way to achieve an automatic mode sorting of the aeroelastic frequencies, making frequency constraints easier to apply. Another limitation of the current work is that spar cap bucking is only taken into account using a simplistic geometric constraint and skin buckling is not considered, since BECAS is currently not capable of modeling non-linear effects. For a description of the key parameters for the DTU 10MW RWT used as the baseline platform in this work please see [18]. As described above, only the rotor is optimized in this work leaving all other parameters unaltered. Although the outer shape is controlled by the optimizer, the cross sectional shape is, as described in Section 3, based on an interpolation between the FFA-W3 airfoil series, and as such, the aerodynamic characteristics of the airfoils are unchanged.

5. Finite Difference Gradient Quality

As mentioned in Section 2 the underlying codes that are used in the framework do not provide analytic gradients, and finite difference is therefore needed to compute the gradient of the

Parameter	# of DVs	**Comment**
Chord	6	-
Twist	5	Root twist fixed
Relative thickness	3	Root and tip relative thickness fixed
Blade prebend	4	-
Blade precone	1	-
Blade length	1	-
Tip-speed ratio	1	-
Trailing edge uniax	2	Pressure/suction side
Trailing edge triax	2	Pressure/suction side
Trailing panel triax	2	Pressure/suction side
Spar cap uniax	4	Pressure/suction side
Leading panel triax	2	Pressure/suction side
Leading edge uniax	2	Pressure/suction side
Leading edge triax	2	Pressure/suction side
DP4	5	Pressure side spar cap position/rear web attachment
DP5	5	Pressure side spar cap position/front web attachment
DP8	5	Suction side spar cap position/front web attachment
DP9	5	Suction side spar cap position/rear web attachment
Total	60	

Table 1. Free form deformation spline (FFD) design variables used in the optimizations.

objective and constraints. The accuracy of the gradients is critical to get a rapidly and smoothly converging optimization, which required careful scaling of all design variables and correct choice of finite difference step size.

Figure 3 shows two examples of gradients computed for the aerostructural workflow; one is the gradient of the objective function (AEP) with respect to the chord design variables, and the other is the blade tip deflection with respect to the spar cap uniax thickness. Both gradients require the fully coupled aerostructural analysis, involving firstly the evaluation of stiffness properties based on the lofted blade shape and material thicknesses followed by the aeroelastic solver evaluating aerodynamic performance and deflections. As is evident neither set of gradients converge fully for decreasing step sizes, although both exhibit fairly smooth convergence. Based on these results all parameters were scaled to match a step size of $dx = 0.01$, corresponding to 1% of the representative scale of the parameters.

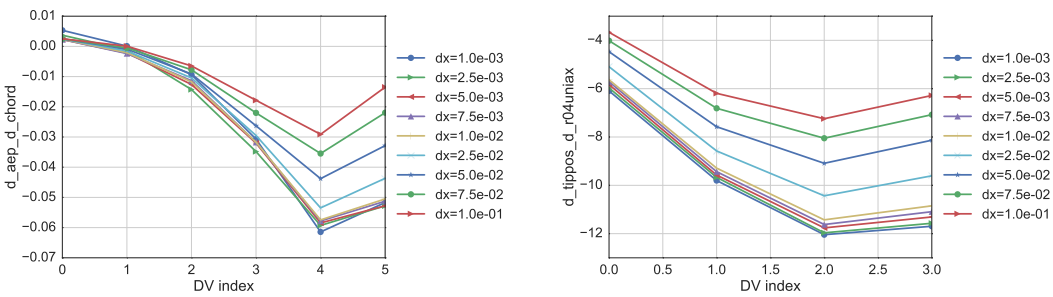

Figure 3. Finite difference gradient evaluations for different step sizes on the quantities AEP wrt chord and blade maximum tip deflection under operation wrt spar cap thickness.

Constraint	Value	**Comment**
max(chord)	< 6.2 m	Maximum chord limited for transport.
max(prebend)	< 6.2 m	Maximum prebend limited for transport.
max(rotor cone angle)	> -5 deg	-
min(relative thickness)	> 0.24	Same airfoil series as used on the DTU 10MW RWT.
min(material thickness)	> 0.0	Ensure FFD splines do not produce negative thickness.
$t/w_{sparcap}$	> 0.08	Basic constraint to avoid spar cap buckling.
min(tip tower distance)	$>$ ref value	DLC1.3 operational tip deflection cannot exceed that of the DTU 10MW RWT.
Blade root flapwise moments (MxBR)	$<$ ref value	DLB loads cannot exceed starting point.
Blade root edgewise moments (MyBR)	$<$ ref value	DLB loads cannot exceed starting point.
Tower bottom fore-aft moments (MxTB)	$<$ ref value	DLB loads cannot exceed that starting point.
Rotor torque	$<$ ref value	Ensure that the rotational speed is high enough below rated to not exceed generator maximum torque.
Blade mass	< 1.01 * ref value	Limit increase in blade mass to maintain equivalent production costs.
Blade mass moment	< 1.01 * ref value	Limit increase in blade mass moment to minimise edgewise fatigue.
Lift coefficient @ $r/R = [0.5 - 1.]$	< 1.35	Limit operational lift coefficient to avoid stall for turbulent inflow conditions.
Ultimate strain criteria	< 1.0	Aggregated material failure in each section for 12 load cases.

Table 2. Non-linear constraints used in the design process.

6. Design Load Cases

The most challenging task in an aerostructural optimization of a wind turbine rotor is to choose the design load cases to run. For a wind turbine the full IEC design load basis can involve over 1000 time series simulations, simulating normal operation, extreme events and fault situations. Evaluating all these cases within an optimization context is not practical with the set of tools used in this work, and a reduced set of cases must therefore be chosen. Another issue is that many of these cases involve turbulent stochastic inflow, which in a gradient based optimization context can lead to poor gradient quality. Pavese et al. [19] have carried out a study to derive equivalent reduced load cases that mimic the full design load basis, but omits using turbulent inflow and only involves key DLCs. In this work, we therefore use a small set of cases, involving DLC1.3, DLC2.1 and DLC6.x, for which cases in DLC1.3 employs a strong shear in place of turbulence to excite the 1P frequency of the rotor with only 150 seconds of simulation time. For more details see [19].

To evaluate tip tower clearance it was found the time domain simulations resulted in poor gradient quality, and a steady state case was therefore used instead representing DLC1.3 with a wind speed of 15 m/s, and zero blade pitch, which was found to drive the design in the desired direction. It was found that designs constrained using this simple flow case subsequently also

stayed within the actual time domain simulations constraint, although actually too conservative.

7. Results

Figure 4 shows the optimized blade planform with chord, twist, relative thickness and prebend shape. The resulting chord distribution results in a slightly more slender blade with the tip extended to a length of 94.3 m. The twist and relative thickness distributions are changed slightly, with most notably an increase in twist towards the tip. The prebend shape was allowed to increase to the same magnitude as the maximum chord, and the optimizer fully exploits this, but interestingly places the prebend primarily towards the tip, where the blade is most loaded and deflects the most.

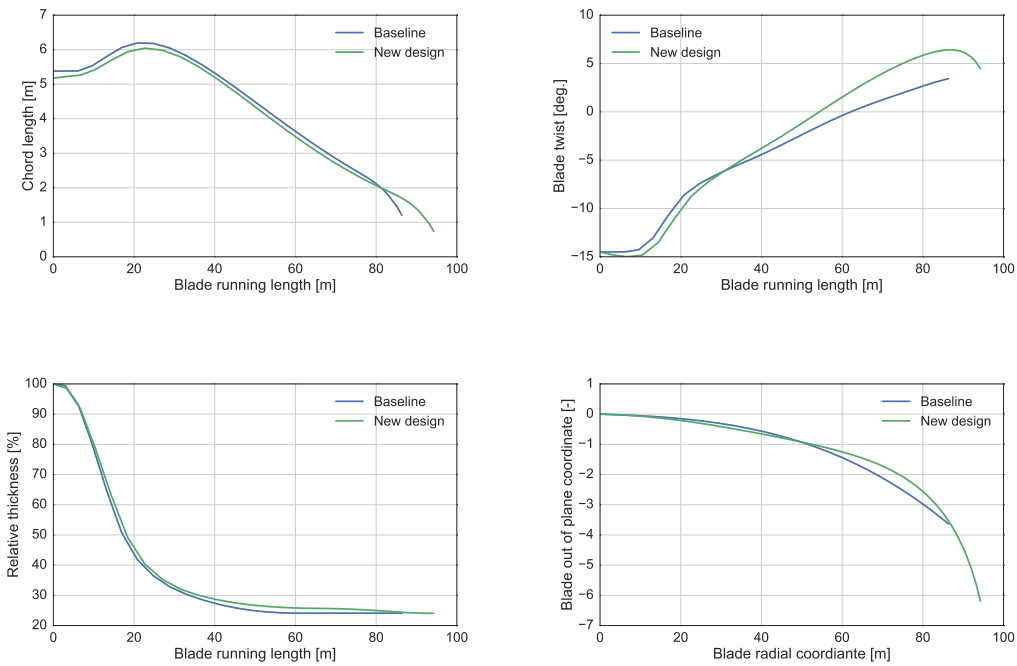

Figure 4. Optimized blade planform compared to the baseline DTU 10MW RWT.

The material stacking sequence for the different regions along the blade is shown in Figure 5. While the trailing and leading edge regions are adjusted slightly, the spar cap thickness distribution is significantly different from that of the DTU 10MW RWT. The caps are generally thicker with significantly more material towards the root to not exceed the blade mass moment and edgewise loads constraints.

Figure 6 shows the blade internal geometry and lofted shape. Interestingly, the main laminates are offset relative to each other with the upper caps moved forward of the pitch axis towards the leading edge. Also, the caps have a slight sweep from max chord towards the tip. Figure 7 shows the steady state blade normal force, thrust coefficient, blade torsion and angle of attack, which shows that the optimized blade is aeroelastically tailored to increase torsion towards feather for increasing wind speed, up to 6 degrees at 11 m/s. This results in an unloading of the tip, that enables the blade to respect the tip deflection constraint, and in turbulent inflow result in significant reductions in both fatigue and extreme loads. At low wind

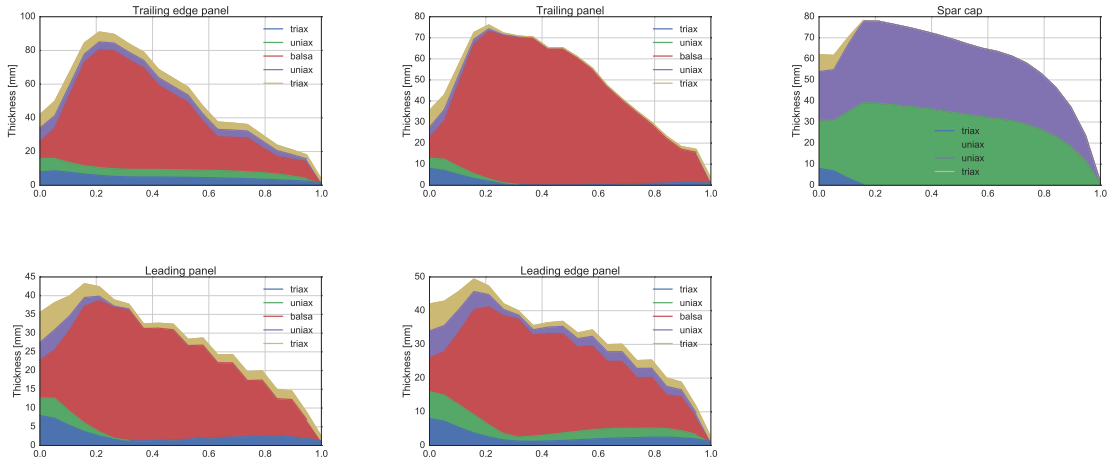

Figure 5. Material stacking sequence for each region along the optimized blade.

speeds the blade thus operates at close to optimal aerodynamic performance with an induction factor of close to 1/3, whereas at higher wind speeds the loading is progressively reduced.

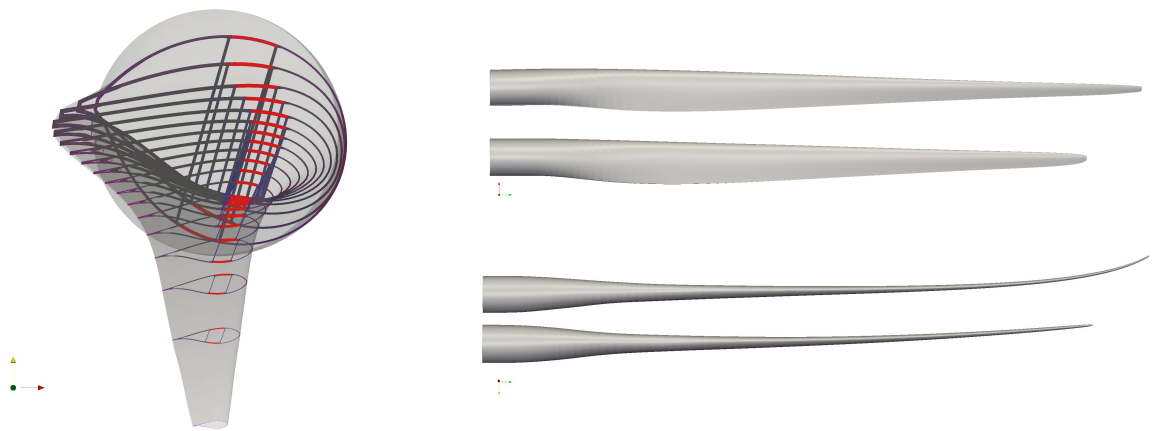

Figure 6. Optimized blade internal structure and lofted shape compared to the baseline DTU 10MW RWT.

Turning to Figure 8 the power curve of the optimized design is plotted against the baseline DTU 10MW RWT, computed with steady state conditions (dotted lines) as well as time domain aeroelastic simulations (fully drawn lines) for a reference turbulence intensity of 10% using six turbulence seeds. The optimized rotor produces 11.1% more AEP than the baseline design assuming Weibull parameters A=8 m/s and k=2, whereas under turbulent inflow conditions the increase in AEP is slightly lower at 8.7%. The right plot in the figure shows the ratio between the steady state and turbulent power curves, where it can be seen that the two rotors behave differently under turbulent flow conditions: Whereas the turbulent mean power below rated is increased by around 5% for the baseline design, the bend twist coupled design lies much closer to the steady state power curve. The torsional coupling in the optimized design thus causes the rotor to shed more power for inflow variations than the baseline design.

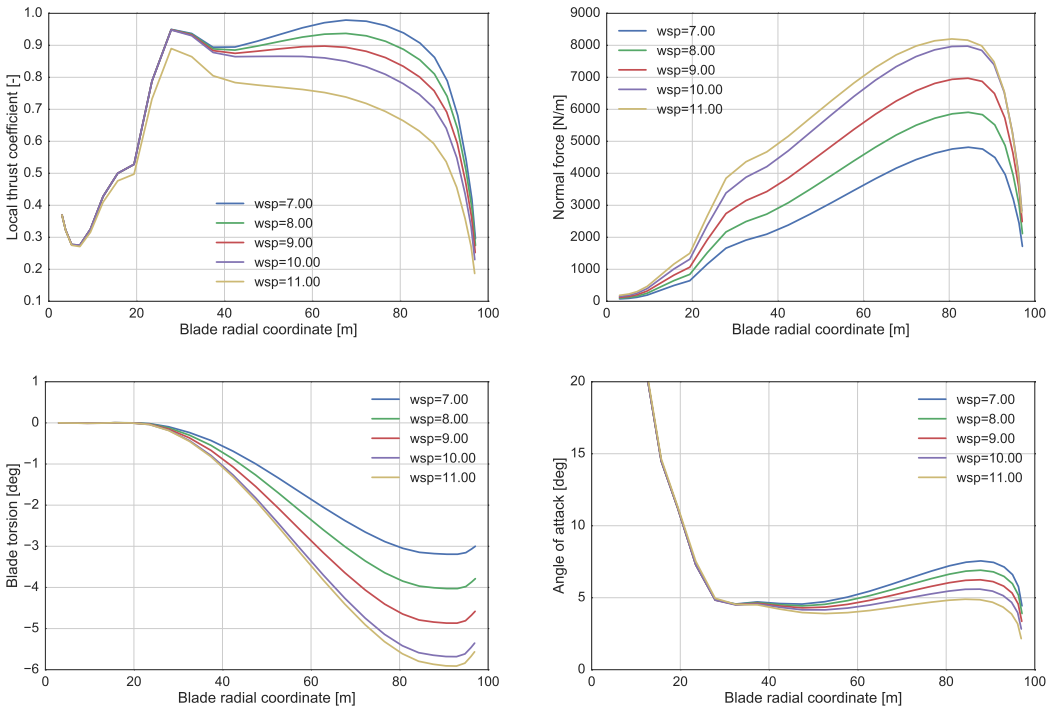

Figure 7. Blade local thrust coefficients and normal forces (upper), and blade torsion and angle of attach (lower) for a range of wind speeds.

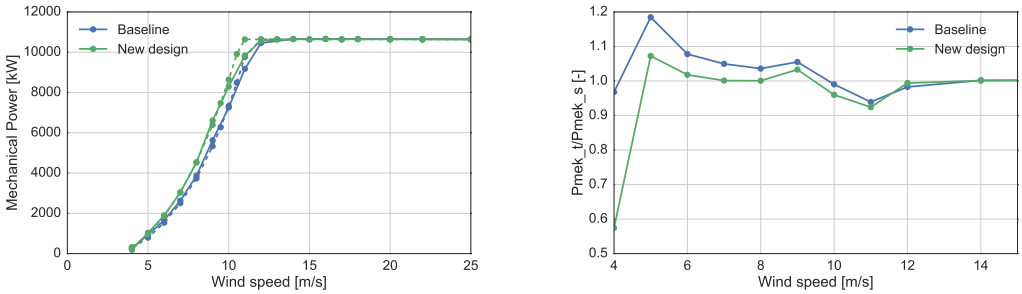

Figure 8. Power curve for the optimized blade compared to the baseline design for steady state conditions (dotted lines) and turbulent power curve with 10% reference TI (left), and the ratio between the turbulent and steady state power curves (right).

Figure 9 shows the turbine lifetime equivalent and extreme loads relative to the baseline DTU 10MW RWT computed using the the full DLB described in [15]. As is evident the tip tower clearance constraint imposed in the design process was conservative compared to the baseline design. The flapwise DEL is reduced by 6% as a result of the blade twisting when subjected to fluctuations in wind speed. Except for blade root torsion fatigue all other sensors are with an acceptable limit of 5% relative to the baseline design, showing that the non-turbulent reduced set of DLCs appears to capture the extreme loads well. However, more advanced methods are

in development to correct the low fidelity DLCs with full fidelity DLCs in an automated design loop, which should converge the optimized design to exactly match constraints of the full set of DLCs.

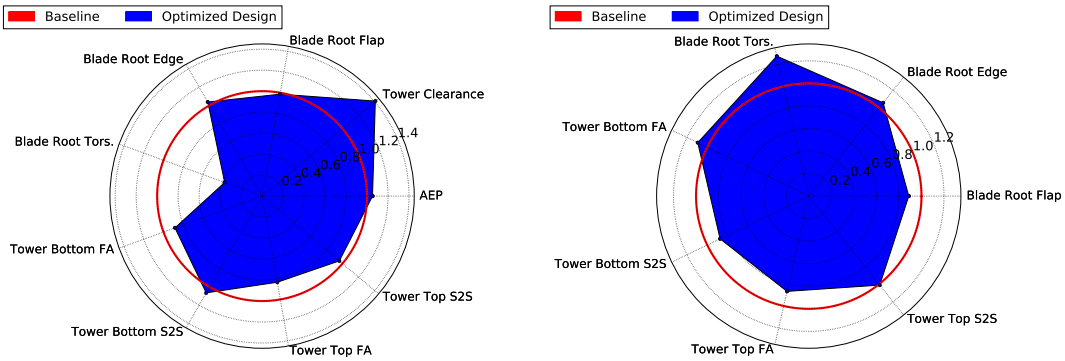

Figure 9. Turbine extreme (left) and lifetime equivalent (right) loads relative to the baseline DTU 10MW RWT computed using the full design load basis described in [15] comprising of 1800 cases.

The structural tailoring that is introduced in the blade is purely achieved through adjustment of the shear center of the blade, and is commonly referred to as shear twist coupling. To achieve the torsionally compliant behaviour of the blade, the torsional stiffness was also reduced in the optimized design by approximately 50% across the main part of the blade. This mechanism is very effective since it does not result in significant reduction of the flapwise stiffness as for example material coupling introduced through off-axis alignment of fibres in the spar cap. And compared to introducing blade sweep, this mechanism also results in a more conventional and thus more easily manufactured outer mold line. Work is still needed to develop the structural design to be manufacturable with conventional techniques, but we are confident that this is achievable without major deterioration of the overall aeroelastic properties of this type of blade.

8. Conclusions

This paper presents an multi-disciplinary wind turbine design framework that is used to design a 10 MW wind turbine rotor for the existing DTU 10MW RWT platform, constrained to the design loads of this platform. The resulting blade is an aeroelastically tailored blade with torsional coupling introduced through geometric tailoring of the internal structure combined with the aerodynamic shape. The optimized blade achieves an increase in AEP of 8.7% relative to the baseline design with extreme and lifetime equivalent loads within 5% except for the blade root torsion fatigue that is increased by 15%. These results clearly demonstrate the power of an integrated multidisciplinary design approach using numerical optimization, in that no previous knowledge of how to achieve the aeroelastic tailoring was included in the optimization problem formulation, but instead purely a result of the optimizer attempting to maximise AEP given a set of design variables and constraints.

Acknowledgments

The research leading to these results has received funding from the European Community's Seventh Framework Programme under grant agreement No. 308974 (INNWIND.EU) and under grand agreement No FP7-ENERGY-2013-1/no 608396 (AVATAR) for which the blade design will be delivered, and the EUDP Stretched Rotor project (J.nr. 64015-0067) within which the

development of the optimization framework used for this work was developed. Finally, the authors would like to acknowledge the dedicated effort of the team behind the development of the OpenMDAO framework which forms an important basis for this work.

References

[1] Fuglsang P, Bak C, Schepers J G, Bulder B, Cockerill T T, Claiden P, Olesen A and van Rossen R 2002 *Wind Energy* **5** 261–279
[2] Bottasso C L, Campagnolo F and Croce A 2012 *Multibody System Dynamics* **27** 21–53 ISSN 1384-5640, 1573-272X
[3] Merz K O 2014 *Wind Energy* n/a–n/a ISSN 1099-1824
[4] Fischer G R, Kipouros T and Savill A M 2014 *Renewable Energy* **62** 506 – 515 ISSN 0960-1481
[5] Andrew Ning S, Damiani R and Moriarty P J 2014 *Journal of Solar Energy Engineering* **136** 041010 ISSN 0199-6231
[6] Zahle F, Tibaldi C, Verelst D, Bak C, Bitsche R and Blasques J 2015 *Aero-Elastic Optimization of a 10 MW Wind Turbine* vol 1 (American Institute of Aeronautics & Astronautics) pp 201–223
[7] 2016 http://openmdao.org
[8] http://pyopt.org/
[9] Wächter A and Biegler L T 2006 *Mathematical Programming* **106** 25–57
[10] Blasques J P and Stolpe M 2012 *Composite Structures* **94** 3278 – 3289 ISSN 0263-8223
[11] http://becas.dtu.dk/
[12] Larsen T J and Hansen A M 2014 How 2 HAWC2, the user's manual Tech. Rep. Risø-R-1597(ver. 4-5)(EN) Risø National Laboratory URL `www.hawc2.dk`
[13] Hansen M H 2004 *Wind Energy* **7** 133–143 ISSN 1099-1824
[14] Tibaldi C, Henriksen L, Hansen M and Bak C 2015 *Wind Energy* ISSN 1095-4244
[15] Hansen M, Thomsen K, Natarajan A and Barlas A 2015 *Design Load Basis for onshore turbines - Revision 00* (Denmark: DTU Wind Energy)
[16] Lambe A B and Martins J R R A 2012 *Structural and Multidisciplinary Optimization* **46** 273–284
[17] http://fusedwind.org/
[18] Bak C, Zahle F, Bitsche R, Kim T, Yde A, Henriksen L C, Andersen P B, Natarajan A and Hansen M 2013 *To be submitted*
[19] Pavese C 2016 *Journal of Physics: Conference Series (Online)* **Accepted**